Analytical Criteria for Magnetization Reversal in a φ_0 Josephson Junction

A.A. Mazanik,[1,2] I.R. Rahmonov,[1,3] A.E. Botha,[4] and Yu.M. Shukrinov[1,4,5,*]

[1] *BLTP, JINR, Dubna, Moscow Region 141980, Russia*
[2] *MIPT, Dolgoprudny, Moscow Region 141700, Russia*
[3] *Umarov Physical Technical Institute, TAS, Dushanbe 734063, Tajikistan*
[4] *Department of Physics, University of South Africa, Florida, Johannesburg 1710, South Africa*
[5] *Dubna State University, Dubna, Moscow Region 141980, Russia*

(Received 6 March 2020; revised 17 May 2020; accepted 20 May 2020; published 1 July 2020)

The switching of magnetization by electric current pulse in the φ_0 Josephson junction formed by ordinary superconductors and a magnetic noncentrosymmetric interlayer is studied. The ground state of this junction is characterized by the finite phase difference φ_0, which is proportional to the strength of the spin-orbit interaction and the exchange field in the normal metal. Based on the Landau-Lifshits-Gilbert and resistively shunted junction model equations we build an analytical description of the magnetization dynamics induced by an arbitrary current pulse. We formulate the criteria for magnetization reversal and, using the obtained results, the form and duration of the current pulse are optimized. The analytical and numerical results are in excellent agreement at $GrI_p \gg 1$, where G is a Josephson-to-magnetic energy ratio, r is a strength of spin-orbit interaction, and I_p is a value of the current pulse. The analytical result allows one to predict magnetization reversal at the chosen system parameters and explains the features of magnetization reversal in the G-r and G-α diagrams, where α is the Gilbert damping. We propose to use such a φ_0 Josephson junction as a memory element, with the information encoded in the magnetization direction of the ferromagnetic layer.

DOI: 10.1103/PhysRevApplied.14.014003

I. INTRODUCTION

The ability to manipulate magnetic properties by the Josephson current and its opposite, i.e., to influence the Josephson current by a magnetic moment, has attracted much recent attention [1–6]. In the superconductor-ferromagnet-superconductor (S-F-S) Josephson junctions, the spin-orbit interaction in a ferromagnet without inversion symmetry provides a mechanism for a direct (linear) coupling between the magnetic moment and the superconducting current. In such junctions, with noncentrosymmetric ferromagnetic interlayer and broken time-reversal symmetry, called φ_0 junctions, the current-phase relation (CPR) is given by $I = I_c \sin(\varphi - \varphi_0)$, where the phase shift φ_0 is proportional to the magnetic moment perpendicular to the gradient of the asymmetric spin-orbit potential [7].

The φ_0 junctions are possible due to the anomalous Josephson effect in different hybrid heterostructures, which reflect the simultaneous interplay of superconductivity, spin-orbit interaction and magnetism [8–22], gives insight into the problem of the mutual influence of superconductivity and ferromagnetism, allows a realization of exotic superconducting states such as the Larkin-Ovchinnikov-Fulde-Ferrell state and triplet ordering. The anomalous Josephson effect promises applications that utilize the spin degree of freedom [13] and demonstrates a number of unique features, important for superconducting spintronics and modern informational technologies. These features allow one to manipulate the internal magnetic moment by using the Josephson current [7,23]. Thus, once the magnetization rotates, a reverse phenomenon should be expected. Namely, magnetization rotation might pump current through the φ_0 phase shift, which is fueled by the term proportional to magnetization and spin-orbit coupling. Such pumping of current leads to the appearance of a dc component in the superconducting current, and plays an important role in the transformation of the I-V characteristics in the resonance region [24].

The application of a dc voltage to the φ_0 junction produces current oscillations, and consequently, magnetic precession. As shown in Ref. [23], this precession may be monitored by the appearance of higher harmonics in the CPR, as well as by the presence of a dc component in the superconducting current. The latter increases substantially near the ferromagnetic resonance (FMR). Konschelle and Buzdin [23] stressed that the magnetic dynamics of the S-F-S φ_0 junction may be quite complicated and strongly

*shukrinv@theor.jinr.ru

anharmonic. In contrast to these results, it was demonstrated in Ref. [24] that precession of the magnetic moment in some current intervals along I-V characteristics may be very simple and harmonic. It is expected that external radiation would lead to a series of interesting phenomena. Among these, there is the possibility of the appearance of half-integer Shapiro steps (in addition to the conventional integer steps) and the generation of an additional magnetic precession at the frequency of the external radiation [23].

Heterostructures that demonstrate the anomalous Josephson effect are being intensively developed. The anomalous Josephson effect was predicted in two types of systems: one with both, spin-orbit interaction and exchange field and another with a noncoplanar magnetization. In Ref. [25] a full microscopic theory to describe the Josephson current through an extended superconductor–normal-metal–superconductor (S-N-S) diffusive junction with an intrinsic spin-orbit coupling (SOC) in the presence of a spin-splitting field h was presented. It was demonstrated that the ground state of the junction corresponds to a finite intrinsic phase difference $0 < \varphi < 2\pi$ between the superconductor electrodes provided that both h and the SOC-induced $SU(2)$ Lorentz force are finite. The authors found the φ_0 as a function of the strengths of the spin fields, the length of the junction, the temperature, and the properties of S-N interfaces. The proper geometry of the system was discussed in Ref. [26], where a quasiclassical transport theory to deal with magnetoelectric effects in superconducting structures was developed. For Josephson junctions the authors establish a direct connection between the inverse Edelstein effect and the appearance of an anomalous phase shift φ_0 in the current-phase relation. In particular they show that φ_0 is proportional to the equilibrium spin current in the weak link.

Predictions of anomalous Josephson junctions with a noncoplanar magnetization have been done in Ref. [27], for ballistic systems, where the anomalous Josephson current appears at zero phase difference in junctions coupled with a ferromagnetic trilayer having noncoplanar magnetizations. The anomalous current was calculated using the Bogoliubov-de Gennes equation, and a clear physical explanation was given of the anomalous Josephson effect in this structure [27]. The authors of Ref. [27] also showed that the triplet proximity correlation and the phase shift in the anomalous current-phase relation all stem from the spin precession in the first and third ferromagnetic layers. In Ref. [28] it was demonstrated that the conditions for the observation of the anomalous Josephson current in diffusive S-F-S junctions are a noncoplanar magnetization distribution and a broken magnetization inversion symmetry of the superconducting current. The authors show that this symmetry can be removed by introducing spin-dependent boundary conditions for the quasiclassical equations at the superconducting-ferromagnet interfaces in diffusive systems [28]. Using this recipe, they then determine the ideal experimental conditions in order to maximize the anomalous current [28].

The Josephson junctions composed of two semiconducting nanowires with Rashba spin-orbit coupling and induced superconductivity from the proximity effect display a geometrically induced anomalous Josephson effect, the flow of a supercurrent in the absence of external phase bias [22]. A generic nonaligned Josephson junction in the presence of an external magnetic field reveals an unusual flux-dependent current-phase relation [20]. Such nonaligned Josephson junctions can be utilized to obtain a ground state other than 0 and π, corresponding to the φ junction, which is tunable via the external magnetic flux. A tunable $\pm\varphi$ and hybrid system between φ and φ_0 junctions were investigated in Refs. [17–19].

Recently, an anomalous phase shift was experimentally observed in different systems, particularly, in the φ_0 junction based on a nanowire quantum dot [29]. A quantum interferometer device was used in order to investigate phase offsets and demonstrate that φ_0 can be controlled by electrostatic gating. The presence of an anomalous phase shift of φ_0 was also experimentally observed directly through CPR measurement in a hybrid S-N-S Josephson junction fabricated using Bi_2Se_3 (which is a topological insulator with strong spin-orbit coupling) in the presence of an in-plane magnetic field [30]. This constitutes a direct experimental measurement of the spin-orbit coupling strength and opens up different possibilities for phase-controlled Josephson devices made from materials with strong spin-orbit coupling. In Refs. [31] and [32], the authors argued that the φ_0 Josephson junction is ideally suited for studying of quantum tunneling of the magnetic moment. They proposed that magnetic tunneling would show up in the ac voltage across the junction and it could be controlled by the bias current applied to the junction. Though the static properties of the S-F-S structures are well studied both theoretically and experimentally, much less is known about the magnetic dynamics of these systems [33–35]. The observation of a tunable anomalous Josephson effect in InAs/Al Josephson junctions measured via a superconducting quantum interference device (SQUID) reported in Ref. [36]. By gate controlling the density of InAs the authors were able to tune the spin-orbit coupling of the Josephson junction by more than one order of magnitude. This gives the ability to tune φ_0, and opens several opportunities for superconducting spintronics [1], and the possibilities for realizing and characterizing topological superconductivity [37–39].

One of the milestones for superconducting electronics, which stands out by ultralow energy dissipation is the creation of cryogenic memory [40–42]. Different realizations for such devices were proposed including devices based on the φ_0 Josephson junctions [41,43–45]. The dc superconducting current applied to a S-F-S φ_0 junction might produce a strong orientation effect on the

ferromagnetic layered magnetic moment [46]. The full magnetization reversal can be realized by applying an electric current pulse [46]. Detailed pictures representing the intervals of the damping parameter α, Josephson to magnetic energy relation G, and the spin-orbit coupling parameter r were obtained with the full magnetization reversal [47]. It was demonstrated that the appearance of the reversal was sensitive to changing the system parameters and showed some periodic structure. Guarcello and Bergeret [45] suggested to use a φ_0 S-F-S junction as a cryogenic memory element, based on the current pulse switching of magnetization proposed in Ref. [46]. In this scheme, a bit of information is associated with the direction of the magnetic moment along or opposite the direction of the easy axis of the ferromagnetic layer. The writing is carried out as a reversal of the magnetic moment by a pulse of current and the readout is performed by detection of the magnetic flux by SQUID inductively coupled to the φ_0 junction. They also explored the robustness of the current-induced magnetization reversal against thermal fluctuations and suggested a way of decoupling the Josephson phase and the magnetization dynamics by tuning the Rashba spin-orbit interaction strength via a gate voltage. A suitable nondestructive readout scheme based on a dc SQUID inductively coupled to the φ_0 junction was also discussed. We stress that in all the above mentioned works the magnetization reversal was studied numerically only.

In our present work we derive an analytical solution for the magnetization dynamics induced by an arbitrary current pulse and formulate the criteria for magnetization reversal in the φ_0 Josephson junctions formed by ordinary superconductors and a magnetic, noncentrosymmetric interlayer. Using the obtained analytical results, we optimize the form and duration of the current pulse. The agreement between analytical and numerical investigations is reached in the case of a large product of the ratio of the Josephson energy to the magnetic energy, strength of spin-orbit interaction and a minimum value of the flowing current. The obtained results explain the periodicity in the appearance of the magnetization-reversal intervals observed in Ref. [47] and allow one to predict magnetization reversal at the chosen system parameters.

The plan of the rest of this work is as follows. In Sec. II we introduce the model and methods, particularly, the derivation of effective field and current pulse. This is followed by Sec. III, where the relation between expressions for the temporal dependence of the current's pulse and the superconducting current is obtained for different Josephson-to-characteristic frequency ratios of the junction. In Sec. IV we present the solution of the Landau-Lifshiz-Gilbert equation for the case when the product of the ratio of the Josephson-to-magnetic energy and spin-orbit coupling is much more that one. Section V is devoted to the small damping regime. We discuss the periodicity in the appearance of the magnetization-reversal intervals in the diagrams "Gilbert damping—Josephson-to-magnetic energy ratio." The periodicity for the diagram "spin-orbit coupling—Josephson-to-magnetic energy ratio" is discussed in Sec. VI. Finally, in Sec. VII we summarize our main results and conclude.

II. MODEL AND METHODS

We study the anomalous Josephson effect in the system with both spin-orbit interaction and exchange field. Such a case was also demonstrated in a recent experiment by Strambini and collaborators [48] who showed that the combined actions of spin-orbit coupling and exchange interaction breaks the phase rigidity of the system, inducing a strong coupling between charge, spin, and superconducting phase.

Here we investigate the system, which consists of a simple φ_0 Josephson junction with planar geometry made up with ordinary superconductors and noncentrosymmetric magnetic interlayer with intrinsic Rashba spin-orbit coupling [23,45,46]. From the microscopic point of view such Rashba coupling is considered as $v_{\mathrm{SO}}\left[\vec{\sigma}\times\vec{p}\right]\cdot\vec{n}$, where $\vec{n}$ is the unit vector along the asymmetric potential gradient and parameter v_{SO} describes its strength. In the following text the microscopical details of the Rashba SOC and exchange field are included in one dimensionless parameter r and the current-phase relation written as $I_s = I_c \sin(\varphi - \varphi_0)$, where $\varphi_0 = rM_y/M_0$, M_y denotes the component of magnetic moment in $\hat{y}$ direction, M_0 is the modulus of the magnetization. So, the physics of S-F-S Josephson structures is determined by the system of equations that consists of the Landau-Lifshits-Gilbert (LLG), resistively shunted junction (RSJ) model with $I_s = I_c \sin(\varphi - \varphi_0)$, and Josephson relation between phase difference and voltage. The dynamics of the magnetic moment in the φ_0 Josephson junction is described by [49]

$$\frac{d\mathbf{M}}{dt} = \gamma_m \mathbf{H}_{\mathrm{eff}} \times \mathbf{M} + \frac{\alpha}{M_0}\left(\mathbf{M}\times\frac{d\mathbf{M}}{dt}\right), \qquad (1)$$

where $\mathbf{M}$ is the magnetization vector, γ_m is the gyromagnetic relation, $\mathbf{H}_{\mathrm{eff}}$ is the effective magnetic field, α is the Gilbert damping parameter, $M_0 = |\mathbf{M}|$.

In order to find the expression for the effective magnetic field we use the model developed in Ref. [23], where it is assumed that the gradient of the spin-orbit potential is along the easy axis of magnetization taken to be along $\hat{z}$. In this case the total energy of the system can be written as

$$E_{\mathrm{tot}} = -\frac{\Phi_0}{2\pi}\varphi I + E_s(\varphi,\varphi_0) + E_M(\varphi_0), \qquad (2)$$

where φ is the phase difference between the superconductors across the junction, I is the external current, $E_s(\varphi,\varphi_0) = E_J\left[1-\cos(\varphi-\varphi_0)\right]$, and $E_J = \Phi_0 I_c/2\pi$ is the Josephson energy. Here Φ_0 is the flux quantum, I_c is

the critical current, $\varphi_0 = l\upsilon_{SO}M_y/(\upsilon_F M_0)$, $l = 4hL/\hbar\upsilon_F$, L is the length of F layer, h is the exchange field of the F layer, $E_M = -K\mathcal{V}M_z^2/(2M_0^2)$, the parameter υ_{SO}/υ_F characterizes a relative strength of spin-orbit interaction, K is the anisotropic constant, and $\mathcal{V}$ is the volume of the ferromagnetic (F) layer.

As mentioned in the Introduction, the physics of the S-F-S Josephson junctions is mostly described by the quasiclassical Green-function method. Here we reduce it to the RSJ model assuming the current-phase relation $I_s = I_c \sin(\varphi - \varphi_0)$, calculated by the Green-function method in Refs. [7], [25], and [26]. We consider a low-frequency regime $\hbar\omega_J \ll T_c$ ($\omega_J = 2eV/\hbar$ being the Josephson angular frequency [50]), which allows us to use the quasistatic approach to treat the superconducting subsystem. If $\hbar\omega_J \ll T_c$, one can use the static value for the total energy of the junction, Eq. (2), considering $\varphi(t)$ as an external potential. Derivative of total energy, Eq. (2), on phase difference gives the current-phase relation, which is used in the RSJ model.

The effective field for the LLG equation is determined by

$$\mathbf{H_{eff}} = -\frac{1}{\mathcal{V}}\frac{\partial E_{\text{tot}}}{\partial \mathbf{M}} = \frac{K}{M_0}\left[Gr\sin\left(\varphi - r\frac{M_y}{M_0}\right)\widehat{\mathbf{y}} + \frac{M_z}{M_0}\widehat{\mathbf{z}}\right], \quad (3)$$

where $r = l\upsilon_{SO}/\upsilon_F$, and $G = E_J/(K\mathcal{V})$.

Using Eqs. (1) and (3), we obtain the system of equations, which describes the dynamics of the magnetization of F layer in S-F-S structure

$$\begin{aligned}
\dot{m}_x &= \frac{1}{1+\alpha^2}\{-m_y m_z + Grm_z\sin(\varphi - rm_y) \\
&\quad - \alpha[m_x m_z^2 + Grm_x m_y\sin(\varphi - rm_y)]\}, \\
\dot{m}_y &= \frac{1}{1+\alpha^2}\{m_x m_z \\
&\quad - \alpha[m_y m_z^2 - Gr(m_z^2 + m_x^2)\sin(\varphi - rm_y)]\}, \\
\dot{m}_z &= \frac{1}{1+\alpha^2}\{-Grm_x\sin(\varphi - rm_y) \\
&\quad - \alpha[Grm_y m_z\sin(\varphi - rm_y) - m_z(m_x^2 + m_y^2)]\},
\end{aligned} \quad (4)$$

where $m_{x,y,z} = M_{x,y,z}/M_0$ satisfy the constraint $\sum_{i=x,y,z} m_i^2(t) = 1$. In this system of equations, time is normalized to the inverse ferromagnetic resonance frequency $\omega_F = \gamma K/M_0 : (t \to t\omega_F)$.

In order to describe the full dynamics of S-F-S structure the LLG equations should be supplemented by the equation for phase difference φ, i.e., the equation of the RSJ model. According to the extended RSJ model [51], which takes into account the derivative of the φ_0 phase shift, the current flowing through the system in the overdamped case is determined by

$$I = \frac{\hbar}{2eR}\left[\frac{d\varphi}{dt} - \frac{r}{M_0}\frac{dM_y}{dt}\right] + I_c\sin\left(\varphi - \frac{r}{M_0}M_y\right), \quad (5)$$

or in the normalized variables,

$$I = w\frac{d\Phi}{dt} + \sin\Phi, \quad (6)$$

where the bias current I is normalized to the critical one I_c and $\Phi = \varphi - rm_y$.

We note that in order to use the same time scale in the LLG and RSJ equations we normalize time to the ω_F^{-1}. In this case an additional parameter given by the $w = \omega_F/\omega_c$ appears, where $\omega_c = 2eI_cR/\hbar$ is a characteristic frequency of the Josephson junction. As we see, the behavior of the system depends on the value of this parameter and it characterizes its different regimes.

The current pulse is $I = I_p$ and it has rectangular form

$$I_p(t) = \begin{cases} A_s, & t \in [t_0, t_0 + \delta t]; \\ 0, & \text{otherwise}, \end{cases} \quad (7)$$

where A_s and δt are the pulse amplitude and width, respectively. We note that if any other form is not specified below, the rectangular form is considered.

The initial conditions for the LLG equation are the $m_x(t=0) = 0$, $m_y(t=0) = 0$, $m_z(t=0) = 1$ and for RSJ-model equation $\varphi(t=0) = 0$. Via the numerical solution [46,47] of Eq. (4), taking into account Eqs. (6) and (7), we obtain the time dependence of magnetization $m_{x,y,z}(t)$, phase difference $\varphi(t)$, and normalized superconducting current $I_s(t) = \sin(\varphi - rm_y)$.

In this paper we also compare the analytical and numerical results concerning the periodicity of magnetization reversal in the α-G and r-G planes. In order to demonstrate the realization of the magnetization-reversal intervals, we solve numerically the system of differential Eqs. (4) and (6) for the fixed values of G and α (or G and r). Then we check the value of m_z at the end of each time domain, and if the reversal is realized, the values of G and α (or r) are recorded to the files. Repeating this procedure for the different values of our parameters we build the figures, which demonstrate the magnetization-reversal appearance in α-G and r-G planes.

III. RELATION BETWEEN $I_p(t)$ AND $\sin\Phi(t)$ AT DIFFERENT w

As mentioned above, the physics of switching in the φ_0 is determined by the LLG equation, Eq. (1), and the RSJ-model equation, Eq. (6). An interesting feature of this system of equations in the overdamped case is a decoupling, i.e., Eq. (6) for Φ is decoupled from the LLG

equation. Eq. (4). This allows us to find the analytical solution for Φ and build the theory for magnetization reversal at some values of model and pulse parameters.

To investigate the magnetization dynamics, we solve Eq. (6) for the pulse $I_p(t)$ and calculate $\sin\Phi$, which is needed to determine the effective magnetic field, Eq. (3). We find that the $\sin\Phi$ profile consists of two regions: the first one is the pumping of the $\sin\Phi$ during the pulse and the second one is the dropping of $\sin\Phi$ to zero when the pulse has been switched off. We investigate these processes in the case of the rectangular pulse, Eq. (7). During the pulse $t_0 \le t \le t_0 + \delta t$, the equation for Φ has a form

$$A_s = w\frac{d\Phi}{dt} + \sin\Phi, \tag{8}$$

with the initial condition $\Phi(t = t_0) = 0$. For $A_s < 1$ it gives

$$\tan\Phi(t)/2 = A_s \frac{\tanh\left[\frac{t-t_0}{\tau_0}\right]}{\tanh\left[\frac{t-t_0}{\tau_0}\right] + \sqrt{1-A_s^2}}. \tag{9}$$

Here $\tau_0^{-1} = \sqrt{1-A_s^2}/2w$, which determines the time scale for approaching a constant value of Φ. So, the formula (9) allows calculation of the $\sin\Phi$ during the pulse $t_0 \le t \le t_0 + \delta t$.

In the second region $t \ge t_0 + \delta t$, when the pulse has been switched off $[I_p(t) = 0]$, we have

$$\sin\Phi(t) = \frac{2\tan\left[\frac{\Phi(t_0+\delta t)}{2}\right]}{\exp\left[\frac{t-t_0-\delta t}{w}\right] + \tan^2\left[\frac{\Phi(t_0+\delta t)}{2}\right]\exp\left[-\frac{t-t_0-\delta t}{w}\right]}, \tag{10}$$

which exponentially drops to zero with a time scale $\tau_1 \sim w$. Here $\tan\{[\Phi(t_0 + \delta t)]/2\}$ is determined by Eq. (9).

We see that there are two physically distinguishable cases. The first case of small w is realized when the conditions $\tau_0 = 2w/\sqrt{1-A_s^2} \ll \delta t$ and $\tau_1 \sim w \ll \delta t$ are fulfilled, i.e., when the pumping time τ_0 and the time τ_1 of dropping to zero, are small in comparison with the pulse duration: $\tau_0 \ll \delta t$ and $\tau_1 \ll \delta t$. These conditions mean that $\sin\Phi$ approaches A_s and drops to 0 for short periods of time τ_0, τ_1, correspondingly, in comparison with the pulse duration δt, thus $\sin\Phi$ shows nearly a rectangular form, which coincides with the pulse $I_p(t)$. This case is demonstrated in Fig. 1(a). Here the magnetic moment feels an approximately constant field $\sin\Phi$ during the pulse.

In the opposite case of $w \gtrsim \tau_0, \tau_1$ the profile of $\sin\Phi$ becomes more complicated. First, the pumping process of $\sin\Phi$ to A_s becomes broader. Second, a significant tail emerges where $I_p(t) = 0$, but $\sin\Phi \ne 0$, which influences the magnetization dynamics. This situation is shown in Fig. 1(b).

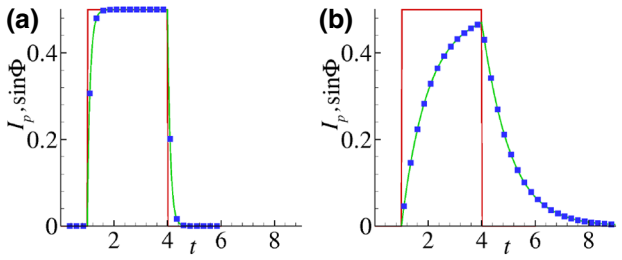

FIG. 1. (a) Dynamics of $\sin\Phi$ (green line), based on the analytical formulas (9) and (10), and numerical solution of Eq. (4) (blue dots). The red line corresponds to the current pulse $I_p(t)$ at $w = 0.1$. The other parameters of calculations are $A_s = 0.5$, $t_0 = 1$, and $\delta t = 3$; (b) the same at $w = 1$.

So, one can notice that parameter w measures time of Φ reaction to the external current. It could be concluded that for small w in comparison with the characteristic time scale of $I_p(t)$ and for arbitrary current pulse $I_p(t)$, where the values are not very close to 1 (to I_c), time derivative $w\dot{\Phi}$ in Eq. (6) can be neglected and then, the relation $\sin\Phi = I_p(t)$ works well.

The following question appears: is magnetization reversal determined by the value of m_z at the end of the current's pulse? The answer is positive for small w only, i.e., when $\omega_F \ll \omega_c$. In this case, when the pulse is switched off, the y component of effective field, Eq. (3), in the LLG equation can be neglected, because $I_p \approx \sin\Phi$. Then, the dynamics of m_z is determined by parameters of the LLG equation: if $m_z < 0$, we observe the magnetization reversal, and it does not happen in the opposite case ($m_z > 0$). At a large value of w the magnetization reversal is determined by the tails in $\sin\Phi$ after switching the pulse off. This feature is demonstrated in Fig. 2, where the influence of $\sin\Phi$ tails on the dynamics of magnetization component m_z is shown at different w.

In the case $w = 0.01$ [see Fig. 2(a)] and the chosen set of parameters we observe the fastest reversal, i.e., the magnetization reversal happens in the current pulse time interval and after switching the pulse off, the $m_z = -1$. In the case of $w = 0.1$, [Fig. 2(b)] the magnetization reversal is also realized, but the value of m_z after switching the pulse off is $m_z = -0.82$ and it reaches the $m_z = -1$ at $t = 40$. At $w = 1$ [Fig. 2(c)], even the value of m_z is positive and has a large enough value at the end of the current pulse ($m_z = 0.5$), we nevertheless observe the magnetization reversal, but it reaches the $m_z = -1$ at $t = 60$ only. The magnetization reversal is not realized at $w = 10$ [Fig. 2(d)] for the chosen values of the system parameters. So, the value of w, i.e., the relation of ω_F to ω_c plays an important role for the magnetization reversal.

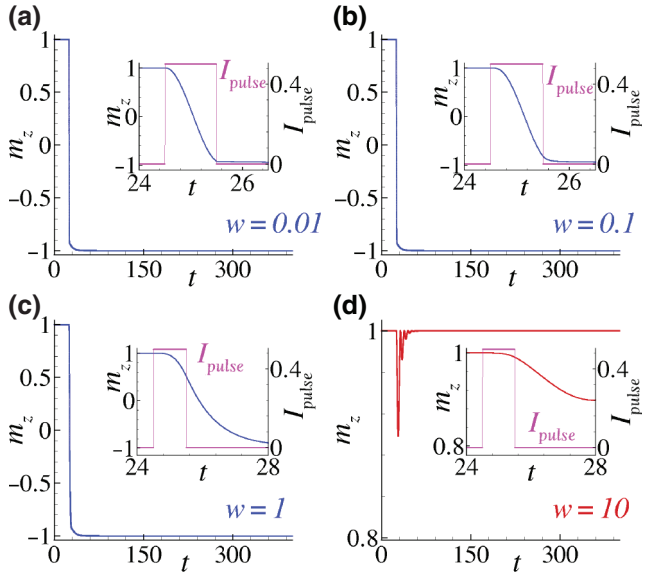

FIG. 2. Time dependence of m_z at $G = 60$, $\alpha = 0.1$, $r = 0.1$, $A_s = 0.5$, and $\delta t = 1$ for different values of parameter w indicated in the figures. Insets demonstrate the enlarged parts showing the m_z dynamics in the time interval around current pulse.

IV. SOLUTION OF THE LLG EQUATION FOR THE $Gr \gg 1$ CASE

Our theory is based on a few key observations. The first one is that for small w and current pulse $I_p(t)$, where the value A_s is not close to 1 (to I_c), as discussed in the previous section, we can neglect the term $w \times d\Phi/dt$ in Eq. (6), which implies the relation

$$I_p(t) = \sin\Phi. \tag{11}$$

The second observation is that the condition $w \ll 1$ can be rewritten as $w = (1/G)(\Phi_0/2\pi V)(\gamma\hbar/2eRM_0) \sim \text{const} \times 1/G \ll 1$. It means that $w \ll 1$ does not imply the case of small $G \ll 1$, therefore we can use the LLG equation in the $Gr \gg 1$ limit as carried out in Ref. [23]. It was also estimated there, that it is plausible for G to vary in a wide range, starting from $G \ll 1$ till $G \sim 100 \gg 1$.

The third observation is that the Gilbert damping can be relatively small $\alpha \ll 1$ [52–54]. So, if the duration of the current pulse is not long, the damping cannot influence the magnetization significantly, and the system may be considered as it is at $\alpha = 0$. Estimations for this case is given in the next section.

According to the previous remarks, using Eq. (11), we can write the LLG equation during the pulse as

$$\begin{cases} \dot{m}_x = Grm_z \sin\Phi = GrI_p(t)m_z, \\ \dot{m}_y = m_x m_z, \\ \dot{m}_z = -Grm_x \sin\Phi = -GrI_p(t)m_x. \end{cases} \tag{12}$$

The limit of the strong coupling $Gr \gg 1$ (but $r \ll 1$) can be treated analytically [23]. In this case $m_y(t) \approx 0$ and for applicability of this method we also need $GrI_p(t) \gg 1$ during the pulse. In the opposite case, zeroes of current pulse $I_p(t)$ destroy the predominance of the used terms and more careful consideration should be carried out. Because $m_y(t) \approx 0$, then $m_x = \rho\sin\phi$, $m_z = \rho\cos\phi$ and we find directly $\dot{\phi} = GrI_p$. So,

$$\phi(t) = Gr\int_{t_0}^{t} dt_1 I_p(t_1). \tag{13}$$

As we see from Eq. (9), after the pulse has been switched off, the $\sin\Phi$ has a fast drop to 0 due to condition $w \ll 1$. In this time region the dynamics of the magnetization is determined only by the interplay of the magnetic anisotropy and the Gilbert damping, which makes the magnetization line up along the easy axis [55].

So, as follows from Eq. (13), the magnetization reversal occurs when

$$\cos\left[Gr\int_{t_0}^{t_0+\delta t} dt_1 I_p(t_1)\right] < 0, \tag{14}$$

where δt is the pulse duration.

We illustrate this idea in Figs. 3(a) and 3(b) for a rectangular pulse $I_p(t) = A_s[\theta(t-t_0) - \theta(t-t_0-\delta t)]$ with $A_s = 0.5$ for two pulse durations $\delta t_1 = 1$ and $\delta t_2 = 3$.

The parameters $G = 100$, $r = 0.1$, $\alpha = 0.005$, $w = 0.01$ are used. In the first case our criteria, Eq. (14), gives $\cos(GrA_s\delta t_1) = 0.28 > 0$, so the reversal is absent, whereas for $\delta t_2 = 3$ we get $\cos(GrA_s\delta t_1) = -0.76 < 0$ and the reversal occurs. We see that the solution, Eq. (13), represented by the blue dashed curve, coincides with the numerical one, represented by the green solid curve, using the complete Eqs. (6) and (1) with Eq. (3) during the pulse. When the pulse has been switched off, the damping destroys any deviations from the easy axis $m_z = \pm 1$. It is demonstrated in the insets to Fig. 3.

It should be noted, that the magnetization reversal is not affected by the form of the current pulse, but by its integral over the pulse duration only. This is demonstrated in Fig. 4(c) for the pulse $I_p(t) = 0.75 - |t - t_0 - t/2|/3$, $\delta t = 3$. The integral $\int dt_1 I_p(t_1)$ for such a pulse is the same as for the pulse in Fig. 3(b), so we see that dynamics of m_z and the magnetization reversal appearance are not different from the case presented in Fig. 3(b).

V. SMALL DAMPING REGIME

It was demonstrated in Ref. [47] by numerical simulations that there was a periodicity in the appearance of intervals of the magnetization reversal under the variation of the spin-orbit coupling, Gilbert damping parameter, and Josephson-to-magnetic energy ratio. Now we can see that

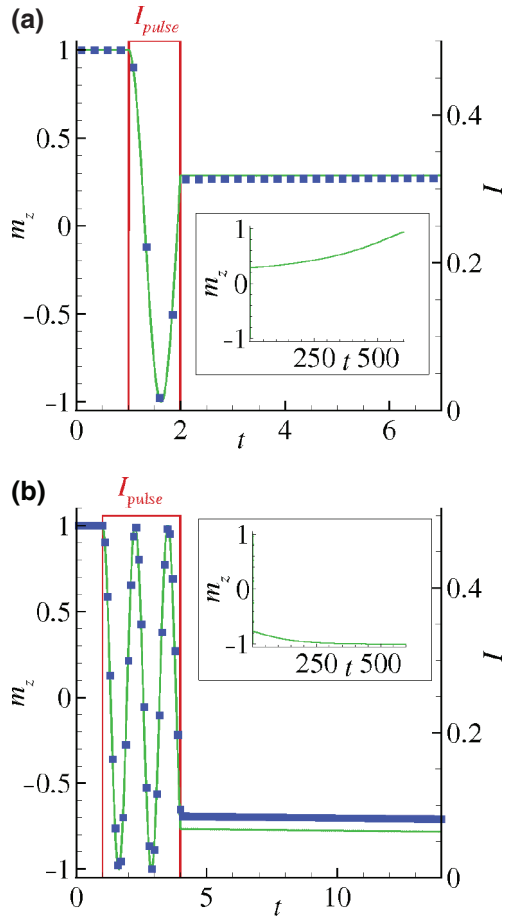

FIG. 3. Dynamics of m_z based on numerical solution of Eqs. (4) and (6) (blue dots) and analytical solutions of Eq. (13) (green line) for different pulse amplitudes and widths. The current pulse is shown by red. The parameters of calculations are $G = 100$, $r = 0.1$, $\alpha = 0.005$, $w = 0.01$, $t_0 = 1$. (a) $A_s = 0.5$, $\delta t = 1$; (b) $A_s = 0.5$, $\delta t = 3$.

the origin of this feature follows from Eq. (14), which leads to such a periodicity by changing parameters of the system and current pulse. As a result, we observe the intervals of parameters with the magnetization reversal and its absence. Based on this equation we can reproduce results of the numerical simulations of Ref. [47] and show the way to optimize magnetization reversal at different conditions. Under current pulse the magnetic moment has complex oscillations determined by system and pulse parameters. Due to the Gilbert damping, the deviated magnetic moment returns back to the stable states with $m_z = 1$ or $m_z = -1$. To describe its dynamics, we write the equation for m_y including the first non-neglecting term in damping parameter α

$$\dot{m}_y = m_x m_z + \alpha G r (1 - m_y^2) \sin \Phi. \tag{15}$$

At the beginning of the pulse $m_y(t) \approx 0$, $m_x m_z$ makes fast oscillations due to $Gr \gg 1$, so rising of m_y is determined

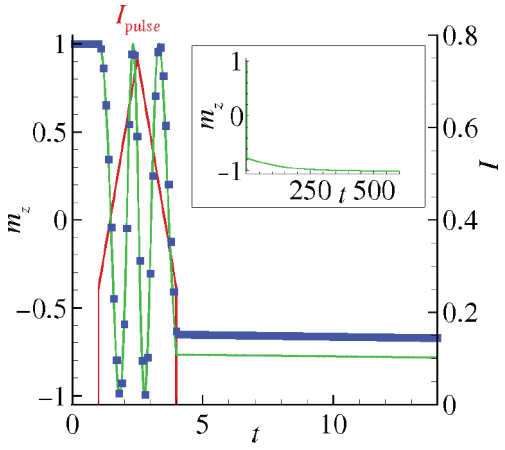

FIG. 4. Dynamics of m_z (green line, analytical; blue dots, numerical) with the current pulse $I_p(t) = 0.75 - |t - t_0 - \delta t/2|/3$, $\delta t = 3$, $\delta t = 3$ (red line). Insets show dynamics after switching current pulse off.

only by the term $\alpha G r \sin \Phi$. For applicability of Eq. (13) we need to keep $m_y(t) \approx 0$, which imposes the condition for the small damping regime

$$\int_{t_0}^{t_0+\delta t} dt_1 \alpha G r \sin \Phi(t_1) = \alpha G r \int_{t_0}^{t_0+\delta t} dt_1 I_p(t_1) \ll 1. \tag{16}$$

For example, at $G = 100$, $r = 0.1$, $A_s/I_c = 0.5$, $\delta t = 3$ we have $\alpha \ll 0.07$, which corresponds to the experimental value of the Gilbert damping parameter [52–54].

According to Eq. (14), the magnetization reversal in the r-G plane under pulse $I_p(t) = A_s[\theta(t - t_0) - \theta(t - t_0 - \delta t)]$ occurs in the hyperbolic areas at

$$\frac{\pi}{2} + 2\pi n \le G_n r A_s \delta t \le \frac{3\pi}{2} + 2\pi n \tag{17}$$

for $n = 0, \pm 1, \ldots$, whereas the most efficient reversal appears when the condition

$$\cos(G r A_s \delta t) = -1 \tag{18}$$

is fulfilled, i.e., $G r A_s \delta t = \pi + 2\pi n$.

Equation (17) does not depend on α, but it indicates the intervals of MR at $\alpha = 0$. These intervals are shown in Fig. 5 by dashed lines. We see that analytical intervals coincide with the numerical ones, calculated at small α. It allows us to make a conclusion that magnetization reversal does not depend on α at its small values.

In order to test the effect of the small damping regime determined by Eq. (16), we calculate numerically the areas in the α-G diagram where the reversal appears. Results are demonstrated in Fig. 5(a).

As we see, in the small damping regime the magnetization reversal does not depend on α. The areas, where it

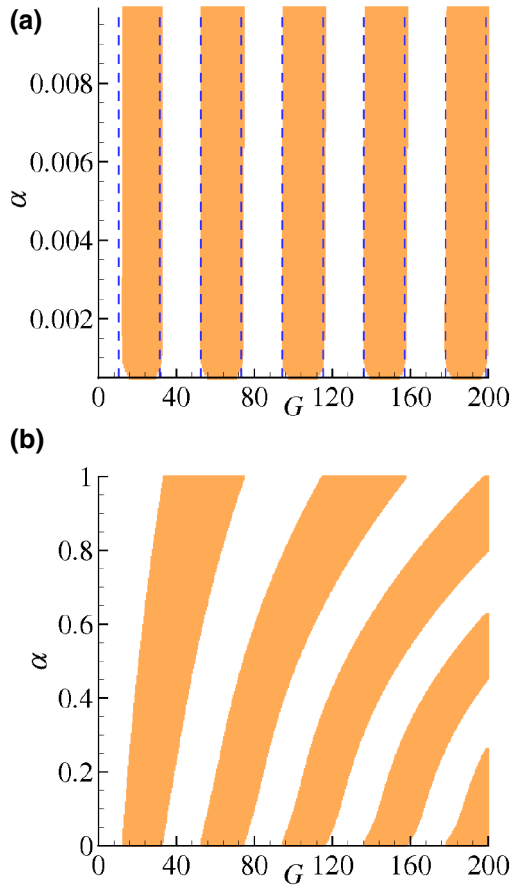

FIG. 5. (a) Comparison of analytical and numerical results demonstrating the periodicity MR realization in the α-G plane at small Gilbert damping. The orange stripes reflect the areas where magnetization reversal is realized. The dashed blue lines correspond to the areas obtained analytically by Eq. (17). The calculation is performed for the G with the step $\Delta G = 0.5$ and for α with the step $\Delta\alpha = 0.0001$. Other parameters are $r = 0.1$, $w = 0.01$, $A_s/I_c = 0.5$, $\delta t = 3$; (b) results of numerical calculations at large Gilbert damping produced with the same parameters.

occurs, are periodic in parameter G, which is determined by Eq. (17). As we see, the realization of the magnetization reversal intervals in α-G plane obtained by numerical simulations at small damping, is in agreement with the analytical results.

Results of numerical calculations of the magnetization reversal intervals in α-G plane at large Gilbert damping produced with the same parameters are demonstrated in Fig. 5(b). We see essential variations of the stripes at large G and α. The estimations made for different S-F-S Josephson junctions show small values of Gilbert damping when our theory works [29,30,36]. Our theory works also in the limit of small Gilbert damping only. Nevertheless, we consider that the presented results are a challenge for future theoretical considerations.

VI. PERIODICITY OF THE MAGNETIZATION REVERSAL IN r-G PLANE

For simplicity we again consider a rectangular pulse in the low damping regime and small w. Equation (17) gives the hyperbolic curves for different n. From a physical point of view they are the curves of a constant amplitude for the driving force in the LLG equation, Eq. (1). In this situation the magnetic moment becomes aligned in the $m_z = -1$ direction exactly after the pulse has been switched off, and the relevant time scale is determined only by the pulse duration, not by the Gilbert damping. It helps us to optimize the pulse duration in order to make the fastest reversal. We see from Eq. (18) that the shortest time is realized for $n = 0$, i.e.,

$$\delta t_{\text{eff}} = \frac{\pi}{GrA_s}. \tag{19}$$

This situation is demonstrated in Fig. 6 for $G = 100$, $r = 0.1$, $\alpha = 0.005$, $w = 0.01$, $A_s = 0.5$, and $\delta t_{\text{eff}} = 0.628$. It leads to the reversal time $\delta t_{\text{rev}} \approx 0.6 \times 10^{-10}$ s for typical $\omega_F \sim 10$ GHz. This time is 2 orders of magnitude smaller than the estimated one in Ref. [46].

Similar hyperbolic profiles of $1/\delta t_{\text{eff}}$ on $I_p(t)$ were obtained theoretically in Ref. [56] and experimentally in Refs. [44] and [57] for a spin-transfer-induced magnetization reversal setup in current-perpendicular spin-valve nanomagnetic junctions. In contrast to our case, this type of setup needs some critical spin-polarized current for magnetization reversal.

In order to test our analytical results, we calculate numerically the areas of the magnetization reversal in the r-G plane, using the complete Eq. (1) with Eqs. (3) and (6). In Fig. 7 we compare them with the analytical results (shown by dashed lines) based on Eqs. (17) and (18).

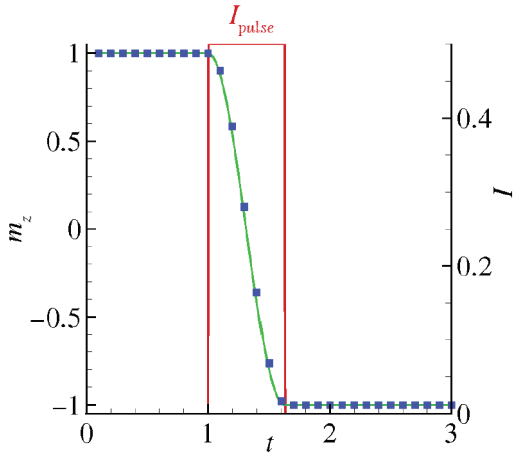

FIG. 6. The same as in Fig. 3 for the current-pulse duration $\delta t_{\text{eff}} = 0.628$ together with analytic according to Eqs. (19). The green line corresponds to the analytical solution and blue dots to the numerical one. The current pulse is shown by the red line.

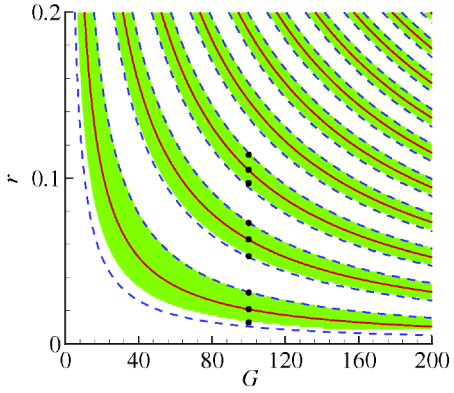

FIG. 7. Periodicity of the magnetization reversal in the r-G plane. Realization of magnetization reversal is shown by the green stripes, the borders of the areas, Eq. (17), by the blue dashed lines and the curves for the most efficient reversal, Eq. (18), by the red lines. The calculation is performed with the step $\Delta G = 0.5$ and step $\Delta r = 0.001$. Other parameters are $\alpha = 0.005$, $w = 0.01$, $A_s/I_c = 0.7$, $\delta t = 3$. The solid lines correspond to the analytical expression (17) with $n = 0, 1, 2, \ldots, 9$. Black circles indicate the point where the dynamics of $m_z(t)$ is shown in Fig. 8.

The almost perfect agreement between numerical and analytical calculations stresses the validity of our theory at the chosen system's parameters. It should be noticed that the periodicity of the magnetization reversal in the r-G plane was observed in Ref. [47] numerically only and for a nongauge-invariant scheme. Comparing both results we may conclude that, actually, the term $\dot{\varphi}_0$ in Eq. (6), which makes the equations gauge invariant, only slightly shifts these areas of magnetization reversal. But, from the other point of view, the gauge-invariant form of equations gives a possibility for analytical consideration of Eq. (6).

Finally, we discuss the magnetization reversal at the parameters corresponding to the different points in the stripes, indicated in Fig. 7. The results of numerical simulations of m_z temporal dependence in the first, second, and third stripes at different values of spin-orbit coupling are shown in Fig. 8.

First we compare the magnetization dynamics for three points in the lowest stripe shown in Figs. 8(a)–8(c). At the boundaries of this stripe we observe a slow reversal, while at the point corresponded to the center of stripe ($r = 0.021$) the magnetization reversal is the fastest one [Fig. 8(b)]. The similar behavior we observe at the points corresponded to the second and the third stripes shown in Fig. 8. The main important difference between dynamics of the m_z in the centers of the different stripes is the following: for the second stripe the m_z makes an additional rotation in compare with a case of the first stripe [see Fig. 8(f)], also for the third stripe m_z makes one more additional rotation [see Fig. 8(i)]. So, it could be directly concluded, that the stripes in Fig. 7 differ from each other by the number of oscillations made by the $m_z(t)$ component during the current pulse.

It should be noted that the obtained periodicity of the magnetization reversal in the S-F-S φ_0 junction is similar to the well-known effect following from the Bloch equations in quantum optics and nuclear magnetic resonance [47,58]. Generally speaking, here we find the limits of parameters, where the famous π pulse is realized in our system. As seen from Figs. 7, 8, and (13), the number of oscillations n made by m_z during the reversal process is proportional to the integral of the pulse function $\int dt I_p(t)$ over time, multiplied by Gr/π. This property takes place for $Gr \gg 1$, $w \ll 1$ and small damping regime, Eq. (16), otherwise the process of the reversal becomes more complicated, as discussed in Ref. [47].

To implement the magnetization-switching element we propose using a memory element that is based on a ferromagnetic anomalous Josephson junction [7]. The latter consists of a S-F-S Josephson junction with a Rashba-like spin-orbit coupling. Its ground state corresponds to a finite phase shift in its current-phase-relation $0 < \varphi_0 < \pi$. In our proposal, the magnetization-switching element is a Josephson junction with a ferromagnetic link, with time-reversal broken intrinsically by the exchange field. As demonstrated theoretically, in these junctions the magnetization of the F layer can be controlled by passing an electric current through the device [23,33,35,46,59,60]. We propose to use such a junction as a memory element with the information encoded in the magnetization direction of the F layer. An important issue for the memory element is the effects stemming from the unavoidable thermal fluctuations on both phase and magnetization dynamics. An exhaustive analysis of the noisy dynamics of a current-biased S-F-S Josephson junction, considering the influence of stochastic thermal fluctuations were presented in Ref. [45] and the robustness of such memory against noise-induced effects was investigated.

Finally, we specify the set of ferromagnetic layer parameters and junction geometry for the possible experimental observation of the predicted effect. In a ferromagnet with weak magnetic anisotropy, as in the permalloy with [61] $K \sim 4 \times 10^{-5}$ KA^{-3}, a junction with a relatively high critical current ($I_c \sim 3 \times 10^5$–5×10^6 A/cm^2), as reported for the Nb/NiGdNi/Nb junction [62], and a ferromagnetic film volume $\mathcal{V} = 10^{-15}$ cm^3, we find that the ratio between the Josephson and the magnetic anisotropy energy to be $G \sim 20$–200 [55]. Another suitable candidate may be the permalloy doped with Pt [63]. As estimated in Ref. [23], if the length of the ferromagnetic layer is of the order of the magnetic decaying length we have $r \sim 0.1$, the value of the parameter Gr is in the range 2–20. Note that ferromagnets without inversion symmetry, like MnSi or FeGe, may also be interesting candidates for the observation of the discussed phenomena.

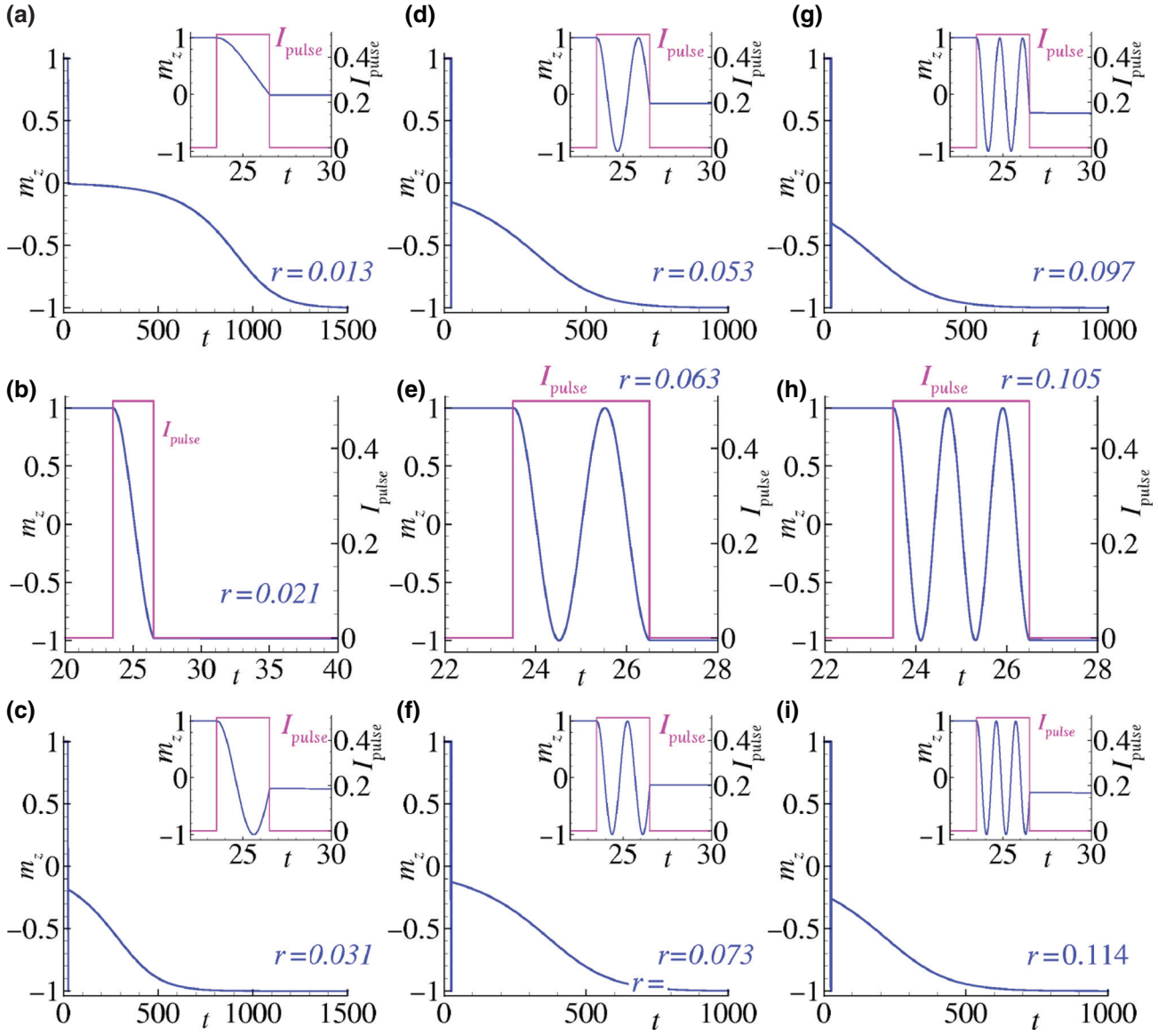

FIG. 8. Results of numerical simulations of m_z temporal dependence in the first stripe (a)–(c), the second stripe (d)–(f), and the third stripe (g)–(i) for the set of parameters $G = 100$, $\alpha = 0.005$ $w = 0.01$, $A_s = 0.5$, $\delta t = 3$, and different value of the SO coupling parameters indicated in the figures.

VII. CONCLUSIONS

The φ_0 Josephson junction is an interesting and important object for superconducting electronics. Its experimental realization opened the way for its use in different applications, particularly, as a cryogenic memory element. In our paper we study the reversal of the magnetic moment in the superconductor-ferromagnet-superconductor φ_0 Josephson junction and developed a theory, which allows us to understand the phenomena of magnetization reversal in this system, and also to predict its occurrence at the chosen system parameters. The analytical criteria for the magnetization reversal are derived in Eqs. (14) and (18), which clarify the dependence of the reversal on the Josephson-to-magnetic energy ratio, spin-orbit coupling, and pulse amplitude, as well as its duration. We compare our analytical results with numerical simulations, explain the observed diagrams G-r and G-α, and demonstrate their almost perfect agreement. We demonstrate the magnetization reversal for different forms of the current pulse. In particular, we find the conditions for faster reversal, which is important for the creation of cryogenic memory, based on this system. We consider that the obtained analytical criteria will be useful in the development of a memory element based on the S-F-S φ_0 Josephson junction.

ACKNOWLEDGMENTS

The reported study is partially funded by the RFBR, Projects 18-02-00318 and 18-52-45011-IND. Sections V and VI of the reported study is funded by the RFBR, Project 20-37-70056. Numerical calculations are made in the framework of the RSF, Project 18-71-10095. Yu.M.S. and A.E.B. gratefully acknowledge support from the University of South Africa's Visiting Researcher Support Program and the SA-JINR collaboration.

[1] J. Linder and J. W. A. Robinson, Superconducting spintronics, Nat. Phys. **11**, 307 (2015).

[2] S. Mai, E. Kandelaki, A. F. Volkov, and K. B. Efetov, Interaction of Josephson and magnetic oscillations in Josephson tunnel junctions with a ferromagnetic layer, Phys. Rev. B **84**, 144519 (2011).

[3] A. I. Buzdin, Proximity effects in superconductor-ferromagnet heterostructures, Rev. Mod. Phys. **77**, 935 (2005).

[4] F. S. Bergeret, A. F. Volkov, and K. B. Efetov, Odd triplet superconductivity and related phenomena in superconductor-ferromagnet structures, Rev. Mod. Phys. **77**, 1321 (2005).

[5] A. A. Golubov, M. Yu. Kupriyanov, and E. Il'ichev, The current-phase relation in Josephson junctions, Rev. Mod. Phys. **76**, 411 (2004).

[6] R. Ghosh, M. Maiti, Yu. M. Shukrinov, and K. Sengupta, Magnetization-induced dynamics of a Josephson junction coupled to a nanomagnet, Phys. Rev. B **96**, 174517 (2017).

[7] A. Buzdin, Direct Coupling between Magnetism and Superconducting Current in the Josephson φ_0 Junction, Phys. Rev. Lett. **101**, 107005 (2008).

[8] T. Yokoyama, M. Eto, and Y. V. Nazarov, Anomalous Josephson effect induced by spin-orbit interaction and Zeeman effect in semiconductor nanowires, Phys. Rev. B **89**, 195407 (2014).

[9] I. V. Krive, A. M. Kadigrobov, R. I. Shekhter, and M. Jonson, Influence of the Rashba effect on the Josephson current through a superconductor/luttinger liquid/superconductor tunnel junction, Phys. Rev. B **71**, 214516 (2005).

[10] A. A. Reynoso, G. Usaj, C. A. Balseiro, D. Feinberg, and M. Avignon, Anomalous Josephson Current in Junctions with Spin Polarizing Quantum Point Contacts, Phys. Rev. Lett. **101**, 107001 (2008).

[11] M. Alidoust and H. Hamzehpour, Spontaneous supercurrent and φ_0 phase shift parallel to magnetized topological insulator interfaces, Phys. Rev. B **96**, 165422 (2017).

[12] M. Alidoust, M. Willatzen, and A.-P. Jauho, Strain-engineered majorana zero energy modes and φ_0 Josephson state in black phosphorus, Phys. Rev. B **98**, 085414 (2018).

[13] V. Braude and Yu. V. Nazarov, Fully Developed Triplet Proximity Effect, Phys. Rev. Lett. **98**, 077003 (2007).

[14] A. Zyuzin, M. Alidoust, and D. Loss, Josephson junction through a disordered topological insulator with helical magnetization, Phys. Rev. B **93**, 214502 (2016).

[15] A. Zyuzin and B. Spivak, Theory of $\pi/2$ superconducting Josephson junctions, Phys. Rev. B **61**, 5902 (2000).

[16] M. Alidoust, Self-biased current, magnetic interference response, and superconducting vortices in tilted weyl semimetals with disorder, Phys. Rev. B **98**, 245418 (2018).

[17] E. Goldobin, D. Koelle, R. Kleiner, and R. G. Mints, Josephson Junction with a Magnetic-Field Tunable Ground State, Phys. Rev. Lett. **107**, 227001 (2011).

[18] E. Goldobin, D. Koelle, and R. Kleiner, Tunable $\pm\varphi$, φ_0, and $\varphi_0 \pm \varphi$ Josephson junction, Phys. Rev. B **91**, 214511 (2015).

[19] R. Menditto, M. Merker, M. Siegel, D. Koelle, R. Kleiner, and E. Goldobin, Evidence of macroscopic quantum tunneling from both wells in a φ Josephson junction, Phys. Rev. B **98**, 024509 (2018).

[20] M. Alidoust and J. Linder, φ-state and inverted Fraunhofer pattern in nonaligned Josephson junctions, Phys. Rev. B **87**, 060503 (2013).

[21] D. S. Shapiro, A. D. Mirlin, and A. Shnirman, Excess equilibrium noise in a topological SNS junction between chiral majorana liquids, Phys. Rev. B **98**, 245405 (2018).

[22] C. Spånslätt, Geometric Josephson effects in chiral topological nanowires, Phys. Rev. B **98**, 054508 (2018).

[23] F. Konschelle and A. Buzdin, Magnetic Moment Manipulation by a Josephson Current, Phys. Rev. Lett. **102**, 017001 (2009).

[24] Yu. M. Shukrinov, I. R. Rahmonov, and K. Sengupta, Ferromagnetic resonance and magnetic precessions in φ_0 junctions, Phys. Rev. B **99**, 224513 (2019).

[25] F. S. Bergeret and I. V. Tokatly, Theory of diffusive φ_0 Josephson junctions in the presence of spin-orbit coupling, Europhys. Lett. **110**, 57005 (2015).

[26] F. Konschelle, I. V. Tokatly, and F. S. Bergeret, Theory of the spin-galvanic effect and the anomalous phase shift φ_0 in superconductors and Josephson junctions with intrinsic spin-orbit coupling, Phys. Rev. B **92**, 125443 (2015).

[27] J.-F. Liu and K. S. Chan, Relation between symmetry breaking and the anomalous Josephson effect, Phys. Rev. B **82**, 125305 (2010).

[28] M. A. Silaev, I. V. Tokatly, and F. S. Bergeret, Anomalous current in diffusive ferromagnetic Josephson junctions, Phys. Rev. B **95**, 184508 (2017).

[29] D. Szombati, S. Nadj-Perge, D. Car, S. Plissard, E. Bakkers, and L. Kouwenhoven, Josephson φ_0-junction in nanowire quantum dots, Nat. Phys. **12**, 568 (2016).

[30] A. Assouline, C. Feuillet-Palma, N. Bergeal, T. Zhang, A. Mottaghizadeh, A. Zimmers, E. Lhuillier, M. Eddrie, P. Atkinson, M. Aprili *et al.*, Spin-orbit induced phase-shift in Bi_2Se_3 Josephson junctions, Nat. Commun. **10**, 1 (2019).

[31] E. M. Chudnovsky, Quantum tunneling of the magnetic moment in the S/F/S Josephson φ_0 junction, Phys. Rev. B **93**, 144422 (2016).

[32] L. Cai and E. M. Chudnovsky, Interaction of a nanomagnet with a weak superconducting link, Phys. Rev. B **82**, 104429 (2010).

[33] X. Waintal and P. W. Brouwer, Magnetic exchange interaction induced by a Josephson current, Phys. Rev. B **65**, 054407 (2002).

[34] V. Braude and Y. M. Blanter, Triplet Josephson Effect with Magnetic Feedback in a Superconductor-Ferromagnet Heterostructure, Phys. Rev. Lett. **100**, 207001 (2008).

[35] J. Linder and T. Yokoyama, Supercurrent-induced magnetization dynamics in a Josephson junction with two

misaligned ferromagnetic layers, Phys. Rev. B **83**, 012501 (2011).

[36] W. Mayer, M. C. Dartiailh, J. Yuan, K. S. Wickramasinghe, E. Rossi, and J. Shabani, Gate controlled anomalous phase shift in Al/InAs Josephson junctions, Nat. Commun. **11**, 1 (2020).

[37] J. Alicea, New directions in the pursuit of majorana fermions in solid state systems, Rep. Prog. Phys. **75**, 076501 (2012).

[38] A. Fornieri, A. M. Whiticar, F. Setiawan, E. Portolés, A. C. Drachmann, A. Keselman, S. Gronin, C. Thomas, T. Wang, R. Kallaher *et al.*, Evidence of topological superconductivity in planar Josephson junctions, Nature **569**, 89 (2019).

[39] H. Ren, F. Pientka, S. Hart, A. T. Pierce, M. Kosowsky, L. Lunczer, R. Schlereth, B. Scharf, E. M. Hankiewicz, L. W. Molenkamp *et al.*, Topological superconductivity in a phase-controlled Josephson junction, Nature **569**, 93 (2019).

[40] Q. P. Herr, A. Y. Herr, O. T. Oberg, and A. G. Ioannidis, Ultra-low-power superconductor logic, J. Appl. Phys. **109**, 103903 (2011).

[41] B. Baek, W. H. Rippard, S. P. Benz, S. E. Russek, and P. D. Dresselhaus, Hybrid superconducting-magnetic memory device using competing order parameters, Nat. Commun. **5**, 1 (2014).

[42] O. A. Mukhanov, Energy-efficient single flux quantum technology, IEEE Trans. Appl. Supercond. **21**, 760 (2011).

[43] N. O. Birge, A. E. Madden, and O. Naaman, in *Spintronics XI* (International Society for Optics and Photonics, Bellingham, WA, 2018), Vol. 10732, p. 107321M.

[44] M.-H. Nguyen, G. J. Ribeill, M. V. Gustafsson, S. Shi, S. V. Aradhya, A. P. Wagner, L. M. Ranzani, L. Zhu, R. Baghdadi, B. Butters *et al.*, Cryogenic memory architecture integrating spin Hall effect based magnetic memory and superconductive cryotron devices, Sci. Rep. **10**, 1 (2020).

[45] C. Guarcello and F. S. Bergeret, Cryogenic Memory Element Based on an Anomalous Josephson Junction, Phys. Rev. Appl. **13**, 034012 (2020).

[46] Yu. M. Shukrinov, I. R. Rahmonov, K. Sengupta, and A. Buzdin, Magnetization reversal by superconducting current in φ_0 Josephson junctions, Appl. Phys. Lett. **110**, 182407 (2017).

[47] P. Kh. Atanasova, S. A. Panayotova, I. R. Rahmonov, Yu. M. Shukrinov, E. V. Zemlyanaya, and M. V. Bashashin, Periodicity in the appearance of intervals of the reversal of the magnetic moment of a ϕ_0 Josephson junction, JETP Lett. **110**, 722 (2019).

[48] E. Strambini, A. Iorio, O. Durante, R. Citro, C. Sanz-Fernández, C. Guarcello, I. Tokatly, A. Braggio, M. Rocci, N. Ligato*et al.*, A Josephson quantum phase battery, arXiv:2001.03393 (2020).

[49] E. M. Lifshitz and L. P. Pitaevskii, *Statistical Physics: Theory of the Condensed State* (Butterworth-Heinemann Ltd, 2013), Vol. 9.

[50] K. K. Likharev and J. E. Lukens, *Dynamics of Josephson Junctions and Circuits* (Gordon and Beach Science Publishers, New York, 1986).

[51] D. S. Rabinovich, I. V. Bobkova, A. M. Bobkov, and M. A. Silaev, Resistive State of Superconductor-Ferromagnet-Superconductor Josephson Junctions in the Presence of Moving Domain Walls, Phys. Rev. Lett. **123**, 207001 (2019).

[52] R. Weber, D.-S. Han, I. Boventer, S. Jaiswal, R. Lebrun, G. Jakob, and M. Kläui, Gilbert damping of CoFe-alloys, J. Phys. D: Appl. Phys. **52**, 325001 (2019).

[53] C. Papusoi, T. Le, C. Lo, C. Kaiser, M. Desai, and R. Acharya, Measurements of Gilbert damping parameter α for CoPt-based and CoFe-based films for magnetic recording applications, J. Phys. D: Appl. Phys. **51**, 325002 (2018).

[54] M. A. Schoen, D. Thonig, M. L. Schneider, T. Silva, H. T. Nembach, O. Eriksson, O. Karis, and J. M. Shaw, Ultra-low magnetic damping of a metallic ferromagnet, Nat. Phys. **12**, 839 (2016).

[55] Yu. M. Shukrinov, A. Mazanik, I. R. Rahmonov, A. E. Botha, and A. Buzdin, Re-orientation of the easy axis in φ_0-junction, Europhys. Lett. **122**, 37001 (2018).

[56] J. Z. Sun, Spin-current interaction with a monodomain magnetic body: A model study, Phys. Rev. B **62**, 570 (2000).

[57] R. H. Koch, J. A. Katine, and J. Z. Sun, Time-Resolved Reversal of Spin-Transfer Switching in a Nanomagnet, Phys. Rev. Lett. **92**, 088302 (2004).

[58] L. Mandel and E. Wolf, *Optical Coherence and Quantum Optics* (Cambridge University Press, Cambridge, 1995).

[59] I. V. Bobkova, A. M. Bobkov, and M. A. Silaev, Spin torques and magnetic texture dynamics driven by the supercurrent in superconductor/ferromagnet structures, Phys. Rev. B **98**, 014521 (2018).

[60] Yu. M. Shukrinov, I. R. Rahmonov, and A. E. Botha, Superconducting spintronics in the presence of spin-orbital coupling, IEEE Trans. Appl. Supercond. **28**, 1 (2018).

[61] A. Yu. Rusanov, M. Hesselberth, J. Aarts, and A. I. Buzdin, Enhancement of the Superconducting Transition Temperature in Nb/permalloy Bilayers by Controlling the Domain State of the Ferromagnet, Phys. Rev. Lett. **93**, 057002 (2004).

[62] J. W. A. Robinson, F. Chiodi, M. Egilmez, G. B. Halász, and M. G. Blamire, Supercurrent enhancement in Bloch domain walls, Sci. Rep. **2**, 1 (2012).

[63] A. Hrabec, F. J. T. Goncalves, C. S. Spencer, E. Arenholz, A. T. N'Diaye, R. L. Stamps, and C. H. Marrows, Spin-orbit interaction enhancement in permalloy thin films by Pt doping, Phys. Rev. B **93**, 014432 (2016).